

MAP, MAC, and Vortex-rings Configurations in the Weinberg-Salam Model*

Rosy Teh[†], Ban-Loong Ng and Khai-Ming Wong

School of Physics, Universiti Sains Malaysia
11800 USM Penang, Malaysia

February 19, 2014

Abstract

We report on the presence of new axially symmetric monopole-antimonopole pairs (MAP) solutions and monopole-antimonopole chains (MAC) solutions of the $SU(2) \times U(1)$ Weinberg-Salam model of electromagnetic and weak interactions when the θ -winding number $n = 1$ and 2 . Vortex-rings start to appear from the MAP and MAC configurations when the winding number $n = 3$. The MAP configurations possess zero net magnetic charge whereas the MAC configurations possess net magnetic charge $4\pi n/e$. In the MAP configurations, when $n = 1$ and 2 , the monopole-antimonopole pair is bounded by the Z^0 field flux string. However, in the MAC configurations there is no string connecting the monopole and the adjacent antimonopole. The MAC configurations possess infinite total energy whereas the MAP configurations possess finite total energy.

1 Introduction

Magnetic monopole was first introduced into the Maxwell theory by P.A.M. Dirac [1]. The presence of the magnetic monopole with pole strength g leads to the requirement that all electric charges have to be quantized in integral multiples of a unit electric charge e given by the formula $\frac{ge}{hc} = \frac{1}{2}n$. The fact that electric charges are quantized and that there are no other explanation for this quantization makes magnet monopole a very important particle that has yet to be discovered. The magnetic field of the Dirac monopole carries a string singularity.

*To be submitted for publication

[†]E-mail: rosyteh@usm.my

In 1969, a non-Abelian magnetic monopole with only a point singularity was found as a solution to the pure SU(2) Yang-Mills theory by Wu and Yang[2]. However both the Dirac and Wu-Yang monopole possess infinite energy due to the presence of a point singularity in the solutions. It was in 1974 that a finite energy magnetic monopole was found by 't Hooft and Polyakov [3] in the SU(2) Georgi-Glashow model. The mass of the 't Hooft-Polyakov monopole was calculated to be of order $137 M_W$, where M_W is the mass of the intermediate vector boson. In the Georgi-Glashow model, $M_W < 53$ GeV, however the mass is given by $M_W = 80.385 \pm 0.015$ GeV in the 2010 Particle Physics Booklet [4]. Hence the mass of the magnetic monopole in the Georgi-Glashow model is of the order of 11 TeV.

A few years later in 1977, Y. Nambu found string-like configurations in the SU(2) \times U(1) Weinberg-Salam model [5]. These configurations are a monopole-antimonopole pair bound by a flux string of the Z^0 field. The total energy of this MAP configuration is finite and the mass of the monopole and antimonopole together with the string is estimated to be in the TeV range. At asymptotically large distances, the real electromagnetic field is a linear combination of U(1) and SU(2) gauge fields created by the MAP. The flux through the string connecting the monopole and antimonopole is U(1) whereas the flux of the monopole and antimonopole is SU(2). Although the arguments and calculations presented are not rigorous, but the existence of massive string-like MAP configurations of the Weinberg-Salam theory had been accurately predicted by Nambu. Our numerical results for the 1-MAP and 2-MAP configurations given in Section 4.3 here confirmed Nambu's finding years ago [5].

Twenty years later, Cho and Maison [6] found the single monopole configuration in the Weinberg-Salam theory. Similar to the Georgi-Glashow model, this configuration is spherically symmetrical. This electrically charged single monopole possesses magnetic charge $4\pi/e$ where e is the electric charge. The apparent string singularity of this monopole along the negative z -axis of the U(1) gauge field is a pure gauge artifact that can be removed with a hypercharge U(1) gauge transformation. Hence unlike the MAP solution discussed by Nambu [5], this monopole does not possess a string. The total energy of this single monopole configuration is infinite due the point magnetic charge of the U(1) field. However by using various method discussed in Ref. [7], this electroweak monopole mass is estimated to be about 4 to 7 TeV which is within the range of the recent MoEDAL detector at LHC, CERN [8]. Hence there is a possibility that this Cho-Maison monopole can be detected by the experiment.

In this paper, we present more numerical monopole configurations that are axially symmetrical. Similar to the Georgi-Glashow theory, the only spherically symmetrical monopole solution is the single monopole with magnetic charge $4\pi/e$ that was found by Cho and Maison [6]. The other monopole configurations are at most axially symmetrical.

We solved the SU(2) \times U(1) Weinberg-Salam equations of motion of the electromagnetic and weak interactions numerically for presence of new axially symmetric

electrically neutral monopole configurations. The solutions found are monopole-antimonopole pairs (MAP) and monopole-antimonopole chains (MAC) configurations when the θ -winding number $n = 1$ and 2. Vortex-ring configurations start to appear from the MAP and MAC configurations when the winding number $n = 3$.

The MAP configurations possess zero net magnetic charge whereas the MAC configurations possess magnetic charge $4\pi n/e$. In the MAP configurations, when $n = 1$ and 2, the monopole-antimonopole pair is bound by the \mathcal{Z}^0 field flux string. However, in the MAC configurations there is no string connecting the monopole and the adjacent antimonopole.

The total energy of these MAC solutions is infinite due the point charge magnetic monopole of the U(1) field as discussed by Cho and Maison [6] for their single 1-monopole solution. Similar to the MAP solution discussed by Nambu [5], the MAP solutions found here possess finite total energy. This is because unlike the MAC solutions, there is no point magnetic charge monopole present in the U(1) field.

In the next Section, we briefly present the Weinberg-Salam model and in Section 3 we obtained the reduced equations of motion by using the axially symmetrical magnetic ansatz. The MAC, MAP, and vortex-ring configurations are discussed in Section 4. When $n = 1$ and 2, the MAC configurations presented are the one pole, three poles, and five poles solutions and the MAP configurations presented are the two poles and four poles solutions. When $n = 3$, vortex-rings configurations are found. We end with some comments in Section 5.

2 The Standard Weinberg-Salam Model

The Lagrangian in the standard Weinberg-Salam model is given by [6], [7]

$$\mathcal{L} = -(\mathcal{D}_\mu \phi)^\dagger (\mathcal{D}^\mu \phi) - \frac{\lambda}{2} \left(\phi^\dagger \phi - \frac{\mu^2}{\lambda} \right)^2 - \frac{1}{4} \mathbf{F}_{\mu\nu} \cdot \mathbf{F}^{\mu\nu} - \frac{1}{4} G_{\mu\nu} G^{\mu\nu}, \quad (1)$$

$$\mathcal{D}_\mu \phi = \left(D_\mu - \frac{ig'}{2} B_\mu \right) \phi, \quad D_\mu = \partial_\mu - \frac{ig}{2} \boldsymbol{\sigma} \cdot \mathbf{A}_\mu, \quad (2)$$

where \mathcal{D}_μ is the covariant derivative of the $SU(2) \times U(1)$ group and D_μ is the covariant derivative of the $SU(2)$ group only. The gauge coupling constant, potentials, and electromagnetic fields of the $SU(2)$ group are given by g , $\mathbf{A}_\mu = A_\mu^a (\frac{\sigma^a}{2i})$, and $\mathbf{F}_{\mu\nu} = F_{\mu\nu}^a (\frac{\sigma^a}{2i})$ respectively, whereas the U(1) group's gauge coupling constant, potentials, and electromagnetic fields are given g' , B_μ , and $G_{\mu\nu}$ respectively. The σ^a are Pauli matrices. The complex scalar Higgs doublet is ϕ , the Higgs field potentials' strength is λ and Higgs field mass is μ . The Higgs field vacuum expectation value is given by $\zeta = \frac{\mu}{\sqrt{\lambda}}$. The metric used is $-g_{00} = g_{11} = g_{22} = g_{33} = 1$.

The equations of motion that follow from Lagrangian (1) are

$$\mathcal{D}^\mu \mathcal{D}_\mu \phi = \lambda (\phi^\dagger \phi - \zeta^2) \phi, \quad (3)$$

$$D^\mu \mathbf{F}_{\mu\nu} = -\mathbf{j}_\nu = \frac{ig}{2} \{ \phi^\dagger \boldsymbol{\sigma} (\mathcal{D}_\nu \phi) - (\mathcal{D}_\nu \phi)^\dagger \boldsymbol{\sigma} \phi \}, \quad (4)$$

$$\partial^\mu G_{\mu\nu} = -k_\nu = \frac{ig'}{2} \{ \phi^\dagger (\mathcal{D}_\nu \phi) - (\mathcal{D}_\nu \phi)^\dagger \phi \}. \quad (5)$$

The Higgs field can also be written as

$$\begin{aligned} \phi &= \Phi \boldsymbol{\xi}, \quad \boldsymbol{\xi}^\dagger \boldsymbol{\xi} = 1, \\ \hat{\Phi}^a &= \boldsymbol{\xi}^\dagger \sigma^a \boldsymbol{\xi}, \quad \sigma^a = \begin{pmatrix} \delta_3^a & \delta_1^a - i\delta_2^a \\ \delta_1^a + i\delta_2^a & -\delta_3^a \end{pmatrix} \end{aligned} \quad (6)$$

where Φ is the Higgs modulus, $\boldsymbol{\xi}$ is a column 2-vector, and $\hat{\Phi}^a$ is the Higgs field unit vector. The energy density of Lagrangian (1) is given by

$$\begin{aligned} \mathcal{E} &= \frac{1}{4} F_{ij}^a F_{ij}^a + \frac{1}{2} F_{i0}^a F_{i0}^a + \frac{1}{4} G_{ij} G_{ij} + \frac{1}{2} G_{i0} G_{i0} + (\mathcal{D}_i \phi)^\dagger (\mathcal{D}_i \phi) \\ &+ (\mathcal{D}_0 \phi)^\dagger (\mathcal{D}_0 \phi) + \frac{\lambda}{2} \left(\phi^\dagger \phi - \frac{\mu^2}{\lambda} \right)^2. \end{aligned} \quad (7)$$

3 The Axially Symmetric Magnetic Ansatz

The axially symmetric magnetic ansatz is given by [9] , [10]

$$\begin{aligned} gA_i^a &= -\frac{1}{r} \psi_1(r, \theta) \hat{n}_\phi^a \hat{\theta}_i + \frac{1}{r} \psi_2(r, \theta) \hat{n}_\theta^a \hat{\phi}_i + \frac{1}{r} R_1(r, \theta) \hat{n}_\phi^a \hat{r}_i - \frac{1}{r} R_2(r, \theta) \hat{n}_r^a \hat{\phi}_i, \\ gA_0^a &= \tau_r(r, \theta) \hat{n}_r^a + \tau_\theta(r, \theta) \hat{n}_\theta^a, \\ g\Phi^a &= \Phi_1(r, \theta) \hat{n}_r^a + \Phi_2(r, \theta) \hat{n}_\theta^a = \Phi(r, \theta) \hat{\Phi}^a, \\ \boldsymbol{\xi} &= i \begin{pmatrix} \sin \frac{\alpha(r, \theta)}{2} e^{-in\phi} \\ -\cos \frac{\alpha(r, \theta)}{2} \end{pmatrix} \\ \hat{\Phi}^a &= \boldsymbol{\xi}^\dagger \sigma^a \boldsymbol{\xi} = -\hat{h}^a. \end{aligned} \quad (8)$$

where the Higgs modulus, $\Phi = \sqrt{\Phi_1^2 + \Phi_2^2}$. In the rectangular coordinate system, the unit vector, [11]

$$\begin{aligned} \hat{h}^a &= h_1(r, \theta) \hat{n}_r^a + h_2(r, \theta) \hat{n}_\theta^a \\ &= \sin \alpha \cos n\phi \delta^{a1} + \sin \alpha \sin n\phi \delta^{a2} + \cos \alpha \delta^{a3}, \\ \cos \alpha &= \{h_1 \cos \theta - h_2 \sin \theta\}, \quad \sin \alpha = \{h_1 \sin \theta + h_2 \cos \theta\} \\ h_1 &= \cos(\alpha - \theta), \quad h_2 = \sin(\alpha - \theta), \quad \alpha = \alpha(r, \theta). \end{aligned} \quad (9)$$

In the MAC, MAP, and vortex-ring solutions, the angle $\alpha(r, \theta) \rightarrow p\theta$ as $r \rightarrow \infty$, where $p = 1, 2, 3, \dots$, is a natural number representing the number of magnetic poles

(monopole/antimonopole) in the configuration. When p is odd, we get the MAC solutions and when p is even, we get the MAP solutions. The spatial spherical coordinate unit vectors are $\hat{r}_i = \sin \theta \cos \phi \delta_{i1} + \sin \theta \sin \phi \delta_{i2} + \cos \theta \delta_{i3}$, $\hat{\theta}_i = \cos \theta \cos \phi \delta_{i1} + \cos \theta \sin \phi \delta_{i2} - \sin \theta \delta_{i3}$, $\hat{\phi}_i = -\sin \phi \delta_{i1} + \cos \phi \delta_{i2}$, whereas the isospin coordinate unit vectors with ϕ -winding number $n = 1, 2, 3, \dots$ are given by

$$\begin{aligned}\hat{n}_r^a &= \sin \theta \cos n\phi \delta_1^a + \sin \theta \sin n\phi \delta_2^a + \cos \theta \delta_3^a, \\ \hat{n}_\theta^a &= \cos \theta \cos n\phi \delta_1^a + \cos \theta \sin n\phi \delta_2^a - \sin \theta \delta_3^a, \\ \hat{n}_\phi^a &= -\sin n\phi \delta_1^a + \cos n\phi \delta_2^a.\end{aligned}\tag{10}$$

The axially symmetric U(1) part of the ansatz is given by

$$g' B_\mu = B_0 \delta_\mu^0 + \frac{1}{r} \mathcal{B}(r, \theta) \hat{\phi}_j \delta_\mu^j.\tag{11}$$

The magnetic ansatz (8) and (11) is substituted into the equations of motion (3) to (5). The equations of motion (3) reduced to the two following partial second order coupled nonlinear equations,

$$\begin{aligned}\partial^i \partial_i \Phi - \lambda(\Phi^2 - \xi^2)\Phi + \frac{1}{4r^2} \{(\mathcal{B} + n \csc \theta)^2 - (n - \psi_2)^2 - (R_2 - n \cot \theta)^2\} \Phi \\ - \frac{1}{4r^2} \left\{ \left(\psi_1 - \left(1 - \frac{\dot{h}_1}{h_2} \right) \right)^2 + \left(R_1 - \frac{r h_1'}{h_2} \right)^2 \right\} \Phi\end{aligned}\tag{12}$$

$$+ \frac{1}{4} \{A_0^2 (g_1 h_2 - g_2 h_1)^2 + [B_0 - A_0 (g_1 h_1 + g_2 h_2)]^2\} \Phi = 0,$$

$$\begin{aligned}\frac{1}{2r^2} \Phi \left\{ \cot \theta - r^2 \left(\frac{\partial^i \partial_i h_1}{h_2} - \frac{\partial^i h_1 \partial_i h_2}{h_2^2} \right) - (\dot{\psi}_1 + \cot \theta \psi_1) + (r R_1)' \right\} \\ + \frac{1}{r^2} \Phi \left\{ r \left(R_1 - \frac{r h_1'}{h_2} \right) (\ln \Phi)' - \left(\psi_1 - \left(1 - \frac{\dot{h}_1}{h_2} \right) \right) (\ln \Phi) \right\} \\ + \frac{1}{2r^2} \Phi (\mathcal{B} + n \csc \theta) (h_1 \psi_2 + h_2 R_2 - n(h_1 + h_2 \cot \theta)) \\ + \frac{1}{2} \Phi B_0 A_0 (g_1 h_2 - g_2 h_1) = 0.\end{aligned}\tag{13}$$

Here ‘‘prime’’ and ‘‘dot’’ mean $\frac{\partial}{\partial r}$ and $\frac{\partial}{\partial \theta}$ respectively. The profile functions of the time component SU(2) gauge potential can be written as $\tau_r = A_0(r, \theta) g_1(r, \theta)$ and $\tau_\theta = A_0(r, \theta) g_2(r, \theta)$ where $g_1^2 + g_2^2 = 1$, and $g_1(r, \theta) \rightarrow h_1$, $g_2(r, \theta) \rightarrow h_2$ at asymptotically large r . The equations of motion (4) reduced to the six following partial second order coupled nonlinear equations,

$$\begin{aligned}
& \partial^i F_{ij}^a + \epsilon^{abc} g A^{bi} F_{ij}^c + \epsilon^{abc} g A^{b0} F_{0j}^c = \\
& \frac{g}{2r} \Phi^2 \left\{ \left(R_1 - \frac{r h'_1}{h_2} \right) \hat{n}_\phi^a \hat{r}_j - \left(\psi_1 - \left(1 - \frac{\dot{h}_1}{h_2} \right) \right) \hat{n}_\phi^a \hat{\theta}_j \right\} \\
& + \frac{g}{2r} \Phi^2 \{ h_2 (R_2 - n \cot \theta) - h_1 (n - \psi_2) \} \hat{h}_\perp^a \hat{\phi}_j \\
& - \frac{g}{2r} \Phi^2 \{ (\mathcal{B} + n \csc \theta) + h_1 (R_2 - n \cot \theta) + h_2 (n - \psi_2) \} \hat{h}^a \hat{\phi}_j, \quad (14)
\end{aligned}$$

$$\begin{aligned}
& \partial^i F_{i0}^a + \epsilon^{abc} g A^{bi} F_{i0}^c = \\
& \frac{g}{2} \Phi^2 \left\{ [A_0 (g_1 h_1 + g_2 h_2) - B_0] \hat{h}^a + A_0 (g_2 h_1 - g_1 h_2) \hat{h}_\perp^a \right\}, \quad (15) \\
& \hat{h}_\perp^a = -h_2 \hat{n}_r^a + h_1 \hat{n}_\theta^a.
\end{aligned}$$

The equations of motion (5) reduced to the two following partial second order coupled nonlinear equations,

$$\begin{aligned}
& \left\{ \left(\partial^i \partial_i - \frac{1}{r^2 \sin^2 \theta} \right) \left(\frac{1}{r} (\mathcal{B} + n \csc \theta) \right) \right\} \hat{\phi}_j \\
& - \frac{g'}{2r} \Phi^2 \{ (\mathcal{B} + n \csc \theta) + (n - \psi_2) h_2 + (R_2 - n \cot \theta) h_1 \} \hat{\phi}_j = 0, \quad (16)
\end{aligned}$$

$$\partial^i \partial_i B_0 - \frac{g'}{2} \Phi^2 \{ B_0 - A_0 (g_1 h_1 + g_2 h_2) \} = 0. \quad (17)$$

There are all together ten reduced electrically charged equations of motion (12)-(17). In the work here, we solved for the electrically neutral monopole configurations by setting A_0 and B_0 to zero and the total number of equations of motions is reduced to only seven equations.

In the electrically neutral monopole configuration, the energy density (7) can be written as

$$\mathcal{E}_n = \frac{1}{4} F_{ij}^a F_{ij}^a + \frac{1}{4} G_{ij} G_{ij} + \partial^i \Phi \partial_i \Phi + \Phi^2 (\mathcal{D}^i \xi)^\dagger (\mathcal{D}_i \xi) + \frac{\lambda}{2} \left(\Phi^2 - \frac{\mu^2}{\lambda} \right)^2, \quad (18)$$

where

$$\begin{aligned}
(\mathcal{D}^i \xi)^\dagger (\mathcal{D}_i \xi) &= \frac{1}{4} \partial^i \alpha \partial_i \alpha + \frac{n^2 (1 - \cos \alpha)}{2r^2 \sin^2 \alpha} + \frac{n}{2} (1 - \cos \alpha) (g' B^i) \partial_i \phi \\
&+ \frac{1}{2} \{ \hat{n}_\phi^a \partial^i \alpha + n \partial^i \phi [\hat{n}_r^a \cos \theta - \hat{n}_\theta^a \sin \theta - \hat{h}^a] \} (g A_i^a) \\
&+ \frac{1}{4} (g A^{ai}) (g A_i^a) - \frac{1}{2} (g' B^i) (g A_i^a) \hat{h}^a + \frac{1}{4} (g' B^i) (g' B_i). \quad (19)
\end{aligned}$$

The energy density (18) can be written as $\mathcal{E}_n = \mathcal{E}_0 + \mathcal{E}_1$. Here $\mathcal{E}_0 = \frac{1}{4} G_{ij} G_{ij}$ is the U(1) part of the energy density and $\mathcal{E}_1 = \mathcal{E}_n - \mathcal{E}_0$ is the part of the energy density

that is regular over all space. The total energy of the MAC configurations is infinite due to \mathcal{E}_0 which is singular at the location of the monopoles. The energy density \mathcal{E}_0 and hence \mathcal{E}_n is however regular over all space for the MAP configurations and the total energy $E_{total} = \frac{1}{4\pi\zeta} \int \mathcal{E}_n d^3x$ is finite. Hence the MAC configurations possess infinite energy whereas the MAP configurations possess finite energy.

In order to determine the electric and magnetic charge of the electromagnetic weak monopole configuration [6], the gauge potentials A_μ^a of Eq. (8) are gauge transformed to $A_\mu^{\prime a}$. Using the gauge transformation,

$$U = -i \begin{bmatrix} \cos \frac{\alpha}{2} & \sin \frac{\alpha}{2} e^{-in\phi} \\ \sin \frac{\alpha}{2} e^{in\phi} & -\cos \frac{\alpha}{2} \end{bmatrix} = \cos \frac{\Theta}{2} + i \hat{u}_r^a \sigma^a \sin \frac{\Theta}{2}, \quad (20)$$

$$\Theta = 3\pi \quad \text{and} \quad \hat{u}_r^a = \sin \frac{\alpha}{2} \cos n\phi \delta_1^a + \sin \frac{\alpha}{2} \sin n\phi \delta_2^a + \cos \frac{\alpha}{2} \delta_3^a,$$

we obtain the transformed Higgs column unit vector and the SU(2) gauge potentials which are respectively given by

$$\xi' = U\xi = \begin{bmatrix} 0 \\ 1 \end{bmatrix}$$

$$gA_\mu^{\prime a} = -gA_\mu^a - \frac{2}{r} \left\{ \psi_2 \sin \left(\theta - \frac{\alpha}{2} \right) + R_2 \cos \left(\theta - \frac{\alpha}{2} \right) \right\} \hat{u}_r^a \hat{\phi}_\mu$$

$$- \partial_\mu \alpha \hat{u}_\phi^a - \frac{2n \sin \frac{\alpha}{2}}{r \sin \theta} \hat{u}_\theta^a \hat{\phi}_\mu \quad (21)$$

$$+ 2 \left\{ \tau_r \cos \left(\theta - \frac{\alpha}{2} \right) - \tau_\theta \sin \left(\theta - \frac{\alpha}{2} \right) \right\} \hat{u}_r^a \delta_\mu^0,$$

or

$$gA_\mu^{\prime 1} = -\frac{1}{r} \cos n\phi \left\{ \psi_2 h_1 + R_2 h_2 - \frac{n \sin \alpha}{\sin \theta} \right\} \hat{\phi}_\mu$$

$$- \frac{1}{r} \sin n\phi (\psi_1 - \partial_\theta \alpha) \hat{\theta}_\mu + \frac{1}{r} \sin n\phi (R_1 + r \partial_r \alpha) \hat{r}_\mu \quad (22)$$

$$+ \{ \tau_r \sin(\alpha - \theta) - \tau_\theta \cos(\alpha - \theta) \} \cos n\phi \delta_\mu^0$$

$$gA_\mu^{\prime 2} = -\frac{1}{r} \sin n\phi \left\{ \psi_2 h_1 + R_2 h_2 - \frac{n \sin \alpha}{\sin \theta} \right\} \hat{\phi}_\mu$$

$$+ \frac{1}{r} \cos n\phi (\psi_1 - \partial_\theta \alpha) \hat{\theta}_\mu - \frac{1}{r} \cos n\phi (R_1 + r \partial_r \alpha) \hat{r}_\mu \quad (23)$$

$$+ \{ \tau_r \sin(\alpha - \theta) - \tau_\theta \cos(\alpha - \theta) \} \sin n\phi \delta_\mu^0$$

$$gA_\mu^{\prime 3} = \frac{1}{r} \left\{ \psi_2 h_2 - R_2 h_1 - \frac{n(1 - \cos \alpha)}{\sin \theta} \right\} \hat{\phi}_\mu$$

$$+ \{ \tau_r \cos(\alpha - \theta) + \tau_\theta \sin(\alpha - \theta) \} \delta_\mu^0. \quad (24)$$

The electromagnetic potential \mathcal{A}_μ and the neutral potential \mathcal{Z}_μ are defined as

$$\begin{aligned}
\begin{bmatrix} \mathcal{A}_\mu \\ \mathcal{Z}_\mu \end{bmatrix} &= \begin{bmatrix} \cos \theta_W & \sin \theta_W \\ -\sin \theta_W & \cos \theta_W \end{bmatrix} \begin{bmatrix} B_\mu \\ A_\mu'^3 \end{bmatrix} \\
&= \frac{1}{\sqrt{g^2 + g'^2}} \begin{bmatrix} g & g' \\ -g' & g \end{bmatrix} \begin{bmatrix} B_\mu \\ A_\mu'^3 \end{bmatrix}
\end{aligned} \tag{25}$$

where $\theta_W = \cos^{-1} \frac{g}{\sqrt{g^2 + g'^2}}$ is the Weinberg angle. For the monopole solutions presented here, the boundary conditions at large r is such that $gA_\mu'^3 \rightarrow g'B_\mu$, hence the neutral potential $\mathcal{Z}_\mu = \frac{1}{\sqrt{g^2 + g'^2}}(-g'B_\mu + gA_\mu'^3) \rightarrow 0$ as $r \rightarrow \infty$ and this neutral \mathcal{Z} field carry zero electric and magnetic charge as expected. The electromagnetic gauge potential can be written as

$$\mathcal{A}_\mu = \frac{1}{e}(g'B_\mu) + \frac{e}{g^2}(gA_\mu'^3 - g'B_\mu). \tag{26}$$

where the electric charge $e = \frac{gg'}{\sqrt{g^2 + g'^2}}$. Therefore $\mathcal{A}_\mu \rightarrow \frac{1}{e}(g'B_\mu)$ when r goes to infinity. Since the boundary conditions for the MAC and MAP solutions are such that $\mathcal{B} \rightarrow -\frac{n(1-\cos\theta)}{\sin\theta}$ and $\mathcal{B} \rightarrow 0$ respectively at r infinity, the MAP configurations possess zero net magnetic charge whereas the MAC configurations possess magnetic charge $q_m = \frac{4\pi n}{e}$. Both MAC and MAP configurations possess electric charge $q_e = \frac{4\pi r^2}{e} \partial_r B_0$.

The electromagnetic dipole moment μ_m of the MAP configurations can also be calculated by using the boundary condition at large r ,

$$\mathcal{A}_i \rightarrow \frac{1}{e}(g'B_i) = \frac{1}{e} \left(\frac{1}{r} \mathcal{B} \hat{\phi}_i \right) = \frac{1}{e} \mathcal{B} \sin \theta \partial_i \phi = -\frac{\hat{\phi}_i}{r \sin \theta} \left(\frac{\mu_m \sin^2 \theta}{r} \right). \tag{27}$$

Hence $r\mathcal{B} = -e\mu_m \sin \theta$ and by plotting the numerical result for $r\mathcal{B}$, we can read the magnetic dipole moment for the MAP solutions in unit of $\frac{1}{e}$ at $\theta = \frac{\pi}{2}$.

4 The MAC, MAP, and Vortex-ring Configurations

The Weinberg-Salam equations of the motions (12)-(17) were solved numerically using the Maple and MATLAB software for MAC, MAP, and vortex-ring configurations. The monopole configurations discussed here are (i) single monopole ($p = 1$), (ii) monopole-antimonopole pair or 1-MAP ($p = 2$), (iii) monopole-antimonopole-monopole or MAM ($p = 3$), (iv) two monopole-antimonopole pairs or 2-MAP ($p = 4$), and (v) MAMAM ($p = 5$) when the ϕ -winding number $n = 1$ and 2. When $n = 3$, vortex-rings are formed from the MAC and MAP configurations.

4.1 Numerical Procedure

We solved the numerical monopole solutions here for all space by solving for the profiles functions, ψ_1 , ψ_2 , R_1 , R_2 , Φ_1 , Φ_2 , and $\mathcal{B} = \mathcal{B}_G - \frac{n(1-\cos\alpha)}{\sin\theta}$. The seven reduced coupled second order partial differential equations of motion (12)-(17) are solved by fixing boundary conditions at small distances ($r \rightarrow 0$), large distances ($r \rightarrow \infty$), and along the z -axis at $\theta = 0$ and π .

The asymptotic solutions at large r are the self-dual solutions [12], [13], which determines the type of monopole configuration,

$$\begin{aligned} \psi_1 &= \dot{\alpha}, \quad \psi_2 = n \left\{ 1 + \frac{\sin(\alpha - \theta)}{\sin\theta} (a \cos\theta + b) \right\} \\ R_1 &= 0, \quad R_2 = n \left\{ \cot\theta - \frac{\cos(\alpha - \theta)}{\sin\theta} (a \cos\theta + b) \right\} \\ \Phi_1 &= \zeta \cos(\alpha - \theta), \quad \Phi_2 = \zeta \sin(\alpha - \theta), \quad \alpha(r, \theta) = p\theta \\ \mathcal{B}_G &= \psi_2 h_2 - R_2 h_1 = \frac{n((a+b) - \cos\alpha)}{\sin\theta} - \frac{na(1 - \cos\theta)}{\sin\theta}, \end{aligned} \quad (28)$$

where the natural number p determines the number of magnetic poles in the monopole configurations. In the MAC configurations, the parameter p is an odd integer, $a = 1$ and $b = 0$. In the MAP configurations, the parameter p is an even integer, $a = 0$ and $b = 1$. The profile function \mathcal{B} vanishes only for the MAP solutions. We solved the equations of motion (12)-(17) when $p = 1, 2, 3, 4, 5$ and the ϕ -winding number $n = 1, 2$, and 3.

The asymptotic solutions at small r are the trivial vacuum solution and is a common boundary condition for all the monopole configurations,

$$\begin{aligned} \psi_1(0, \theta) &= \psi_2(0, \theta) = R_1(0, \theta) = R_2(0, \theta) = 0, \\ \sin\theta \Phi_1(0, \theta) &+ \cos\theta \Phi_2(0, \theta) = 0, \\ \frac{\partial}{\partial r} \{ \cos\theta \Phi_1(r, \theta) &- \sin\theta \Phi_2(r, \theta) \} \Big|_{r=0} = 0, \\ \mathcal{B}(0, \theta) &= \mathcal{B}_G(0, \theta) = 0. \end{aligned} \quad (29)$$

The common boundary condition along the z -axis at $\theta = 0$ and π for all the monopole configurations is

$$\partial_\theta \psi_1 = \partial_\theta \psi_2 = R_1 = R_2 = \partial_\theta \Phi_1 = \Phi_2 = \mathcal{B} = \mathcal{B}_G = 0. \quad (30)$$

The monopole solutions were solved numerically using the mathematical software, Maple and MATLAB, by fixing the boundary conditions (28) - (30) when $r = 0$, $r = \infty$, $\theta = 0$, and $\theta = \pi$ [10], [12], [13]. As in Ref. [12], and [13], we did not applied the gauge fixing condition, $r\partial_r R_1 - \partial_\theta \psi_1 = 0$ onto the monopole solutions here. Using the finite difference approximation method, the seven reduced equations of motion (12) - (17) were converted into a system of nonlinear

equations which is then discretized onto a non-equidistant grid of size 70×60 covering the integration regions $0 \leq \bar{x} \leq 1$ and $0 \leq \theta \leq \pi$. The compactified coordinate $\bar{x} = \frac{r}{r+1}$. Upon replacing the partial derivative $\partial_r \rightarrow (1 - \bar{x})^2 \partial_{\bar{x}}$ and $\frac{\partial^2}{\partial r^2} \rightarrow (1 - \bar{x})^4 \frac{\partial^2}{\partial \bar{x}^2} - 2(1 - \bar{x})^3 \frac{\partial}{\partial \bar{x}}$, the Jacobian sparsity pattern of the system was constructed by using Maple. The system of nonlinear equations is then solved numerically by MATLAB using the constructed Jacobian sparsity pattern, the trust-region-reflective algorithm, and a good initial starting solution. The overall error in the numerical results is estimated at 10^{-4} .

4.2 MAC/Vortex-ring Configurations

The MAC solutions obtained are the single n -monopole ($p = 1, n = 1, 2, 3$), the monopole-antimonopole-monopole or MAM ($p = 3, 3$ poles), and the MAMAM ($p = 5, 5$ poles) when the θ -winding number $n = 1$ and 2 . When $n = 3$, vortex-rings are formed. In both the MAM and MAMAM configurations, two vortex-rings together with one monopole are formed when $n = 3$. The profiles functions, $\psi_1, \psi_2, R_1, R_2, \Phi_1, \Phi_2$, and \mathcal{B}_G for the MAC solutions are obtained numerically and they are all regular and bounded functions of r and θ .

The Higgs field modulus Φ for the MAC configurations are shown in Figure 1 by 3-D plot and contour line plot along the x - z plane. Figure 1 (a) and (b) show the Higgs field modulus plots for the one monopole solutions when $n = 2$ and 3 respectively. Figure 1 (c) and (d) show the Higgs field modulus plots for the MAM solutions when $n = 1$ and 3 and Figure 1 (e) and (f) show the Higgs field modulus plots for the MAMAM solutions when $n = 1$ and 3 respectively. The locations of the magnetic monopoles and vortex-rings are read from the zeros of the Higgs field modulus and tabulated in Table 1 as $d_{(\rho,z)} = (\rho_i, \pm z_i)$. The Higgs field modulus for the MAC/vortex-ring configurations are almost similar to those of the SU(2) Georgi-Glashow model and there is no string or zero line of the Higgs field connecting the monopole and adjacent antimonopole.

The magnetic dipole moments μ_m for all the MAC configurations are expected to be zero and this confirm by the numerical results, that is $\mu_m = 0$ for both the SU(2) and U(1) magnetic fields [10], [16].

The U(1) and SU(2) magnetic field lines for the one monopole configurations are shown in Figure 2 when $n = 2$ and 3 . There is a one monopole in both the U(1) field and SU(2) field but the monopole is absent in the \mathcal{Z}^0 field. Figure 3 and 4 show the U(1) and SU(2) magnetic field lines of the MAM and MAMAM configurations respectively when $n = 1, 2$, and 3 . Similar to the one monopole configurations of Figure 2, the monopoles and vortex-rings that are found in the SU(2) field are also found in the U(1) field and there are no monopoles or vortex-rings in the \mathcal{Z}^0 field.

Similar to the MAM and MAMAM configurations of the SU(2) Georgi-Glashow model when the θ -winding number $n = 3$, two vortex-rings with center located along the z -axis ($\pm z_i$) and radius ρ_i are formed [9]. In the MAC configurations, the monopoles and vortex-rings are found only in the \mathcal{A}_μ electromagnetic gauge

field, there is no monopole or vortex-ring presents in the neutral \mathcal{Z}_μ gauge field.

The total energy of the MAC configurations is infinite due to the presence of point magnetic charge in the U(1) field. The energy density \mathcal{E}_0 blows up at the locations of the point magnetic charge in the U(1) field. Hence the mass of these monopole can only be estimated as was done for the one monopole solution when $n = 1$ in Ref. [7]. The estimated mass of the one monopole was found to be about 4 to 7 TeV and there is a possibility that this monopole can be detected by the MoEDAL detector in CERN.

4.3 MAP/Vortex-ring Configurations

The MAP solutions obtained are the 1-MAP ($p = 2$, 2 poles) and the 2-MAP ($p = 4$, 4 poles) configurations when the θ -winding number $n = 1$ and 2. When $n = 3$, one vortex-ring is formed in the 1-MAP configuration and two vortex-rings are formed in the 2-MAP configuration just as in the SU(2) Georgi-Glashow model [9]. As in the Section 4.2, the profiles functions, ψ_1 , ψ_2 , R_1 , R_2 , Φ_1 , Φ_2 , and \mathcal{B} for the MAP solutions are obtained numerically and they are all regular and bounded functions of r and θ .

The 3-D and contour line plots of the Higgs field modulus Φ along the x - z plane for the MAP configurations are shown in Figure 5 when $p = 2$, and 4 and when $n = 1, 2$, and 3. The locations of the magnetic monopoles and vortex-rings are read from the zeros of the Higgs field modulus and tabulated in Table 1. There is however a major difference in the Higgs field modulus here compared to the SU(2) Georgi-Glashow model. The Higgs field modulus is not only zero at the locations of the magnetic monopoles but also vanishes along a line of finite thickness connecting the monopole to the adjacent antimonopole. These observations are not surprising as they are in line with the theoretical predictions of Nambu [5] some 37 years ago.

The magnetic field lines of the Abelian U(1) field, the non-Abelian SU(2) field, the neutral \mathcal{Z}^0 field, and the electromagnetic \mathcal{A}_μ field are shown in Figure 6 and 7 for the 1-MAP configuration when $n = 1$ and 3 respectively and in Figure 8 and 9 for the 2-MAP configuration when $n = 1$ and 3 respectively. Unlike the MAC configurations, there is no monopole or vortex-ring found in the Abelian U(1) field. The monopole and antimonopole pairs and vortex-rings are found only in the non-Abelian SU(2) gauge field and hence in the electromagnetic gauge field \mathcal{A}_μ as well as in the neutral \mathcal{Z}^0 field. The SU(2) magnetic field lines of the 1-MAP configuration resemble the magnetic field lines of a bar magnet and those of the 2-MAP configuration resemble the magnetic field lines of two bar magnets. In the U(1) gauge field, there is totally no magnetic pole or vortex-ring but only tubes of magnetic flux going through the location of the MAP.

The total energy of the MAP configurations is finite due to the fact that there is no point magnetic charge presence in the U(1) field. The energy density \mathcal{E}_n is regular and bounded for the MAP configurations. The total energy of these MAP configurations is tabulated in Table 2. Nambu has estimated the energy scale to be in the TeV range [5].

The magnetic dipole moments μ_m in unit of $\frac{1}{e}$ for all the MAP configurations are calculated numerically [10], [16] and the results are tabulated in Table 2.

$d_{(\rho,z)}$	$n = 1$	$n = 2$	$n = 3$
$p = 3$	$(0, 0), (0, \pm 3.375)$	$(0, 0), (0, \pm 2.236)$	$(0, 0), (1.424, \pm 1.283)$
$p = 5$	$(0, 0), (0, \pm 3.559),$ $(0, \pm 6.737)$	$(0, 0), (0, \pm 2.561),$ $(0, \pm 4.914)$	$(0, 0),$ $(1.690, \pm 2.928)$
$d_{(\rho,z)}$	$n = 1$	$n = 2$	$n = 3$
$p = 2$	$(0, \pm 2.202)$	$(0, \pm 1.063)$	$(1.692, 0)$
$p = 4$	$(0, \pm 1.581),$ $(0, \pm 5.435)$	$(0, \pm 1.251),$ $(0, \pm 3.166)$	$(1.606, \pm 1.693)$

Table 1: Table of monopole's and vortex-ring's positions, $d_{(\rho,z)} = (\rho_i, \pm z_i)$, when $\lambda = 1$.

5 Comments

Other interesting solutions of the Weinberg-Salam equations include the electrically neutral and charged sphalerons, antisphalerons, and vortex-rings configurations, [14] and [15]. These sphalerons solutions are finite energy solutions that were solved using the axially symmetric magnetic ansatz of the SU(2) group. Unlike the monopole solutions of the Weinberg-Salam equations, they possess finite energy because there is no magnetic monopole presents in these configurations. In the monopole solutions, the Higgs field defines a nontrivial mapping from the two-sphere at r infinity to the trivial vacuum manifold as $r \rightarrow 0$, while for the sphaleron solutions this mapping is trivial. Hence unlike the monopoles, sphalerons are classical static solutions that do not possess topological magnetic charge but are unstable configurations that represent the top of the energy barrier between topologically inequivalent vacua.

In the work here, we present genuine axially symmetric monopole solutions. The MAC solutions given here are the one pole ($p = 1$) M, three poles ($p = 3$) MAM, and five poles ($p = 5$) MAMAM solutions when the θ -winding, $n = 1$, and 2. When $n = 3$, two vortex-rings and one monopole are formed in the $p = 3$ and $p = 5$ solutions. These MAC solutions possess zero magnetic dipole moment μ_m . The monopoles and vortex-rings are both present in the SU(2) and U(1) gauge fields and hence in the electromagnetic gauge field but not in the neutral Z^0 field. The total energy is infinite as the energy density of the point magnetic charge blows up in the U(1) gauge field. There is no string connecting a monopole and its adjacent antimonopole in the MAC configurations. The mass of the monopole

μ_m	$n = 1$	$n = 2$	$n = 3$
$p = 2$	1.339	2.595	4.229
$p = 4$	2.717	5.156	7.435
E_0	$n = 1$	$n = 2$	$n = 3$
$p = 2$	0.059	0.136	0.199
$p = 4$	0.121	0.309	0.513
E_1	$n = 1$	$n = 2$	$n = 3$
$p = 2$	2.548	4.261	5.797
$p = 4$	4.814	7.887	11.772
E_{total}	$n = 1$	$n = 2$	$n = 3$
$p = 2$	2.608(2.60), [2.366]	4.398 (5.60), [4.861]	5.996 (8.36), [6.916]
$p = 4$	4.935 (5.15), [4.655]	8.197 (10.97), [9.471]	12.285 (16.22), [13.749]

Table 2: Table of values of magnetic dipole moment μ_m in unit of $\frac{1}{e}$ and total energy, $E_{total} = \frac{1}{4\pi\zeta} \int \mathcal{E}_n d^3x$, for the MAP solutions when $\lambda = 1$. The values of the total energy given in round bracket are the values provided by Ref. [9] for the corresponding Georgi-Glashow model MAP configurations. The values in square brackets are the values obtained from our numerical calculations for the corresponding Georgi-Glashow model MAP configurations.

in the $SU(2) \times U(1)$ Weinberg-Salam model has been estimated by Cho et al. to be about 4 to 7 TeV [7].

The MAP configurations are different from the MAC configurations as no magnetic monopole or vortex-ring are present in the $U(1)$ gauge field and hence there is no point magnetic charge. Therefore the MAP configurations possess finite total energy. In the MAP configurations, each monopole-antimonopole pair is bound by the \mathcal{Z}^0 flux string and the electromagnetic field lines pattern of a MAP resembles that of a bar magnet. Our results confirmed the theoretical predictions made by Nambu that there exist string-like configurations in which a pair of monopoles are bound by a flux string of the \mathcal{Z}^0 field [5]. In the MAC configurations, monopole and antimonopole are not bound by the \mathcal{Z}^0 flux string.

The total energy E_{total} in unit of $4\pi\zeta$ of the Weinberg-Salam model MAP configuration is comparable to that of the corresponding Georgi-Glashow model MAP configuration as given in Table 2. In general the position of the monopoles and vortex-rings of the electroweak model does not differ much from that of the corresponding $SU(2)$ Georgi-Glashow model monopole configurations. However a general pattern observed is that the Weinberg-Salam model MAP separation are larger than the corresponding Georgi-Glashow model MAP separation.

The monopole configurations studied here are electrically neutral. Hence further work are done by setting the electric charge profile functions, A_0 and B_0 of the magnetic ansatz (8) and (11) to be nonvanishing. This work on the MAC, MAP and vortex-ring dyons of the $SU(2) \times U(1)$ Weinberg-Salam model will be reported in our next paper.

Acknowledgements

The authors would like to thank the Ministry of Science, Technology and Innovation for the ScienceFund Grant (account number: 305/PFIZIK/613613) and the Ministry of Higher Education for the Fundamental Research Grant Scheme (FRGS).

We would also like to thank Prof. Y.M. Cho for enlightening and encouraging us to pursue this project.

References

- [1] P.A.M. Dirac, Pro. Royal London Soc. Series **A 133**, 60 (1931); Phys. Rev. **74**, 817 (1948).
- [2] T.T. Wu and C.N. Yang, *Properties of Matter under Unusual Conditions*, edited by H. Mark and S. Fernbach (Wiley, New York, 1969) 349; Nucl. Phys. **B 107**, 365 (1976); Phys. Rev. **D 16**, 1018 (1977).
- [3] G. 't Hooft, Nucl. Phys. **B79**, 276 (1974); A.M. Polyakov, JETP Lett. **20**, 194 (1974).
- [4] J. Beringer et al. (Particle Data Group), Phys. Rev. **D 86**, 010001 (2012).
- [5] Y. Nambu, Nucl. Phys. **B 130**, 505 (1977); Int. J. Theor. Phys. **17** (1978) 287.
- [6] Y.M. Cho and D. Maison, Phys. Lett. **B391**, 360 (1997).
- [7] Y.M. Cho, Kyoungtae Kimm, and J.H. Yoon, *Finite Energy Electroweak Dyon*, hep-ph/1305.1699v1 (2013); *Mass of the Electroweak Monopole*, hep-ph/1212.3885v5 (2013).
- [8] J. Pinfold, Rad. Meas. **44**, 834 (2009); CERN Courier **52**, No. 7, p. 10 (2012).
- [9] B. Kleihaus and J. Kunz, Phys. Rev. **D 61**, 025003 (1999); B. Kleihaus, J. Kunz, and Y. Shnir, Phys. Lett. **B570**, 237 (2003); Phys. Rev. **D 68**, 101701 (2003); Phys. Rev. **D 70**, 065010 (2004); J. Kunz, U. Neemann and Y. Shnir, Phys. Lett. **B640**, 57 (2006).
- [10] K.G. Lim, Rosy Teh and K.M. Wong, J. Phys. G: Nucl. Part. Phys. **39** (2012) 025002.
- [11] Rosy Teh, B.L. Ng, and K.M. Wong, Int. J. Mod. Phys. **A28**, 1350144 (2013).
- [12] Rosy Teh, K.M. Wong and K.G. Lim, Int. J. Mod. Phys. **A25**, 5731 (2010).
- [13] Rosy Teh, P.Y. Tan, and K.M. Wong, Int. J. Mod. Phys. **A27**, 1250148, (2012).

- [14] B. Kleihaus, J. Kunz, and M. Leißner, Phys. Lett. **B663**, 438 (2008); Phys. Lett. **B678**, 313 (2009).
- [15] R. Ibadov, B. Kleihaus, J. Kunz, and M. Leißner, Phys. Lett. **B686**, 298 (2010); Phys. Rev. **D82**, 125037 (2010).
- [16] Rosy Teh, B.L. Ng, and K.M. Wong, J. Phys. G: Nucl. Part. Phys. **40**, 035004 (2013).

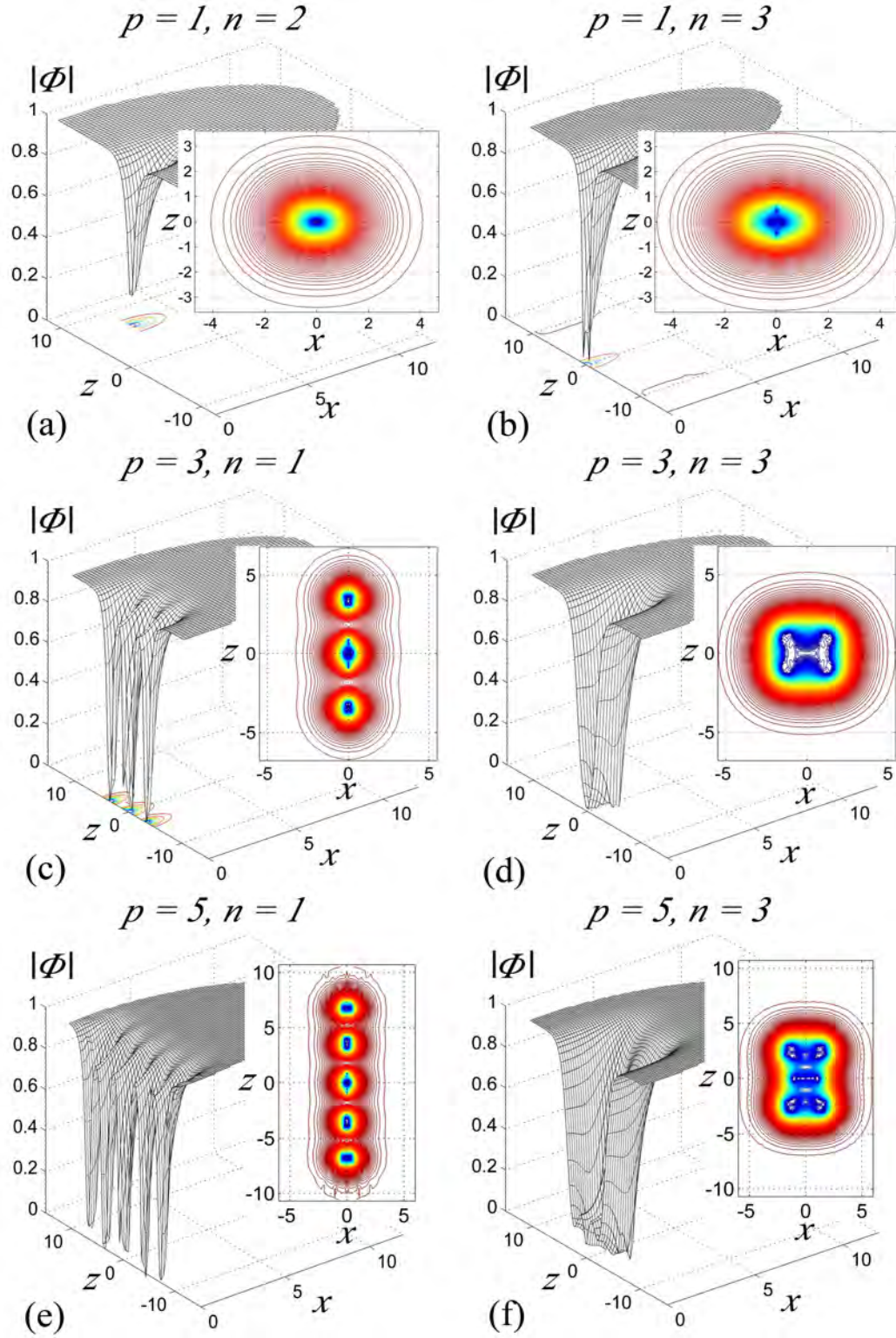


Figure 1: 3-D and contour line plot of the Higgs field modulus Φ along the x - z plane for the one monopole solutions when (a) $n = 2$ and (b) $n = 3$, for the MAM solutions when (c) $n = 1$ and (d) $n = 3$, and for the MAMAM solutions when (e) $n = 1$ and (f) $n = 3$.

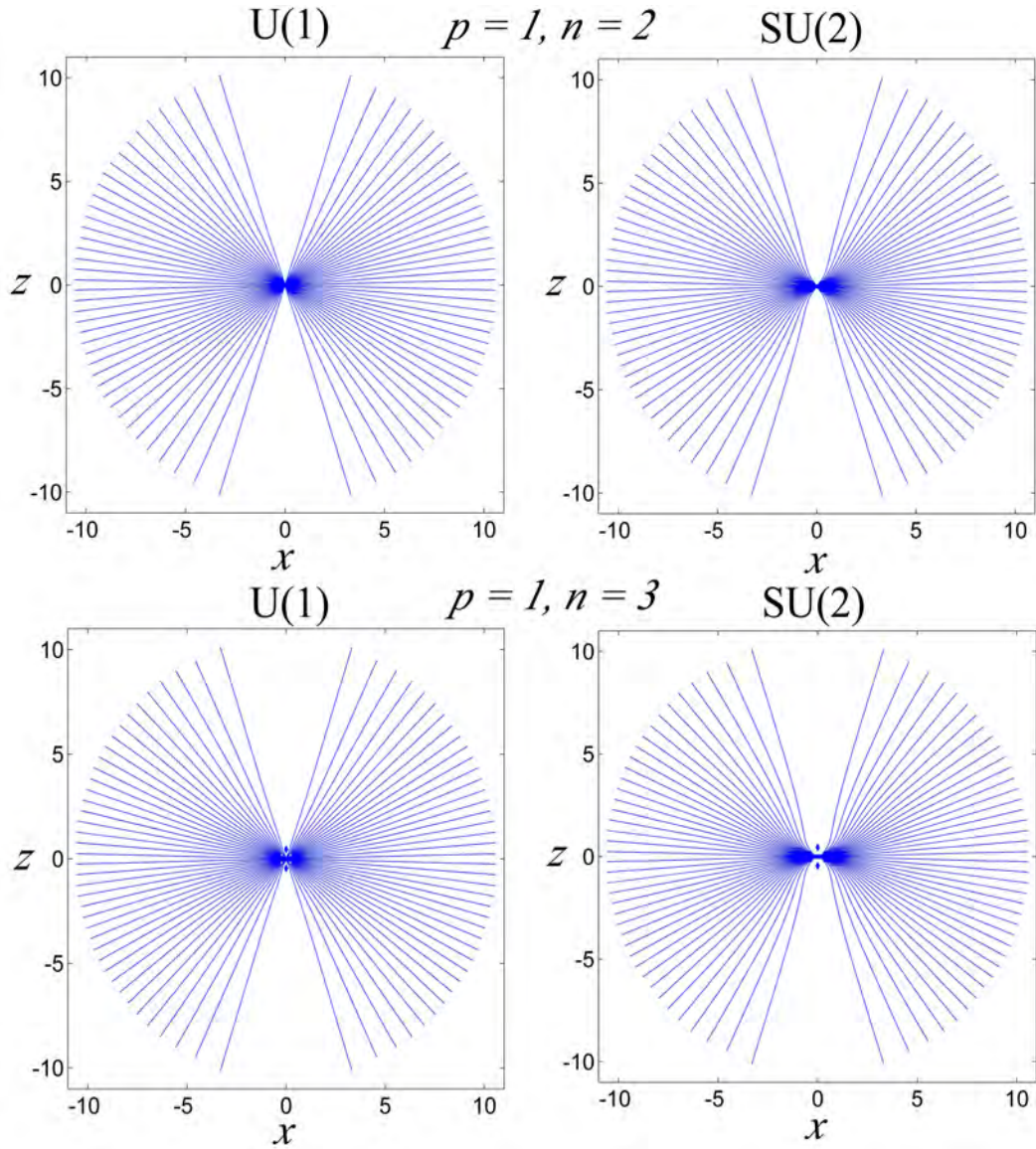


Figure 2: The contour line plot of the U(1) and SU(2) magnetic field lines for the one monopole configurations along the x - z plane when $n = 2$ and 3.

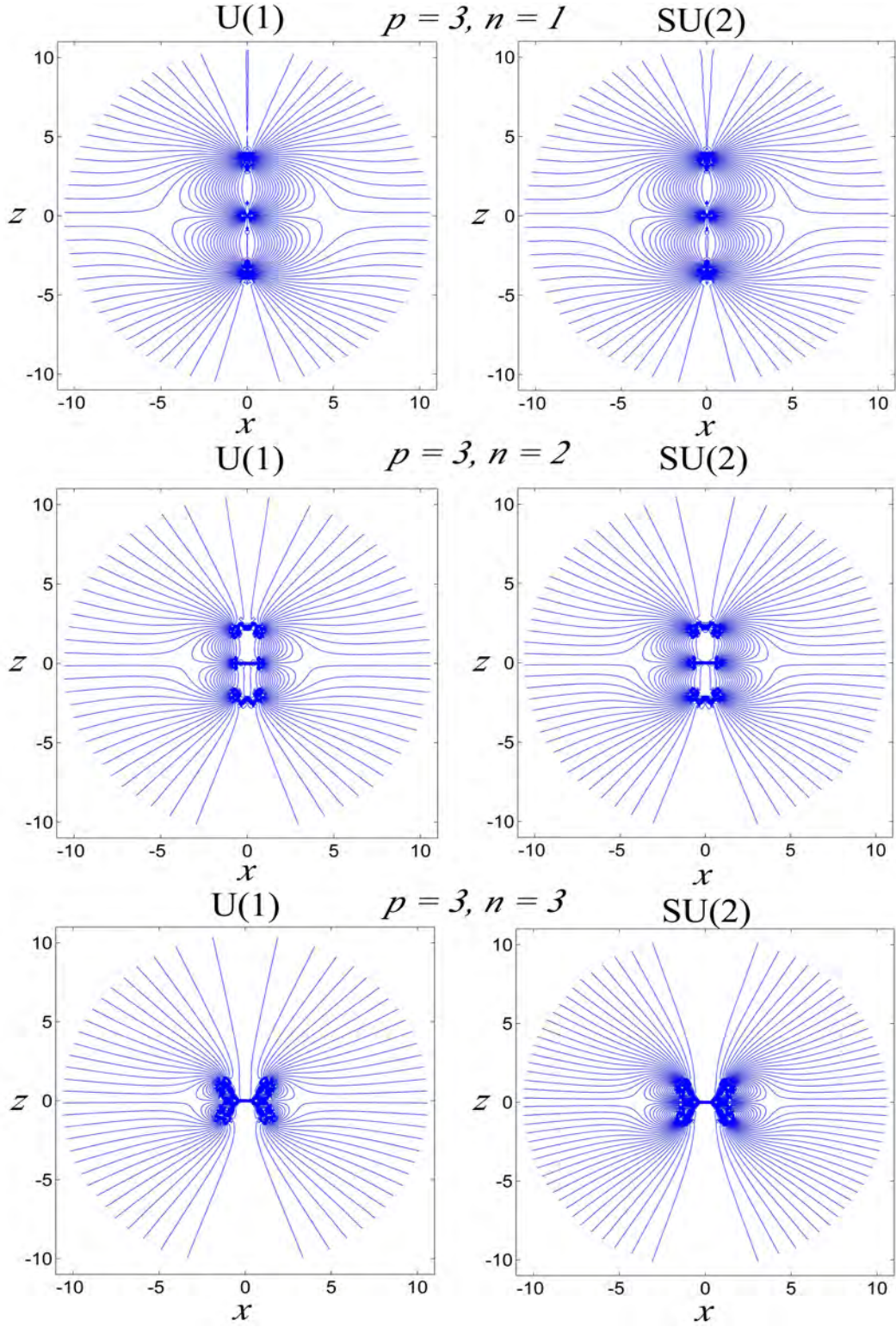


Figure 3: The contour line plot of the $U(1)$ and $SU(2)$ magnetic field lines for the MAM configurations along the x - z plane when $n = 1, 2$ and 3 .

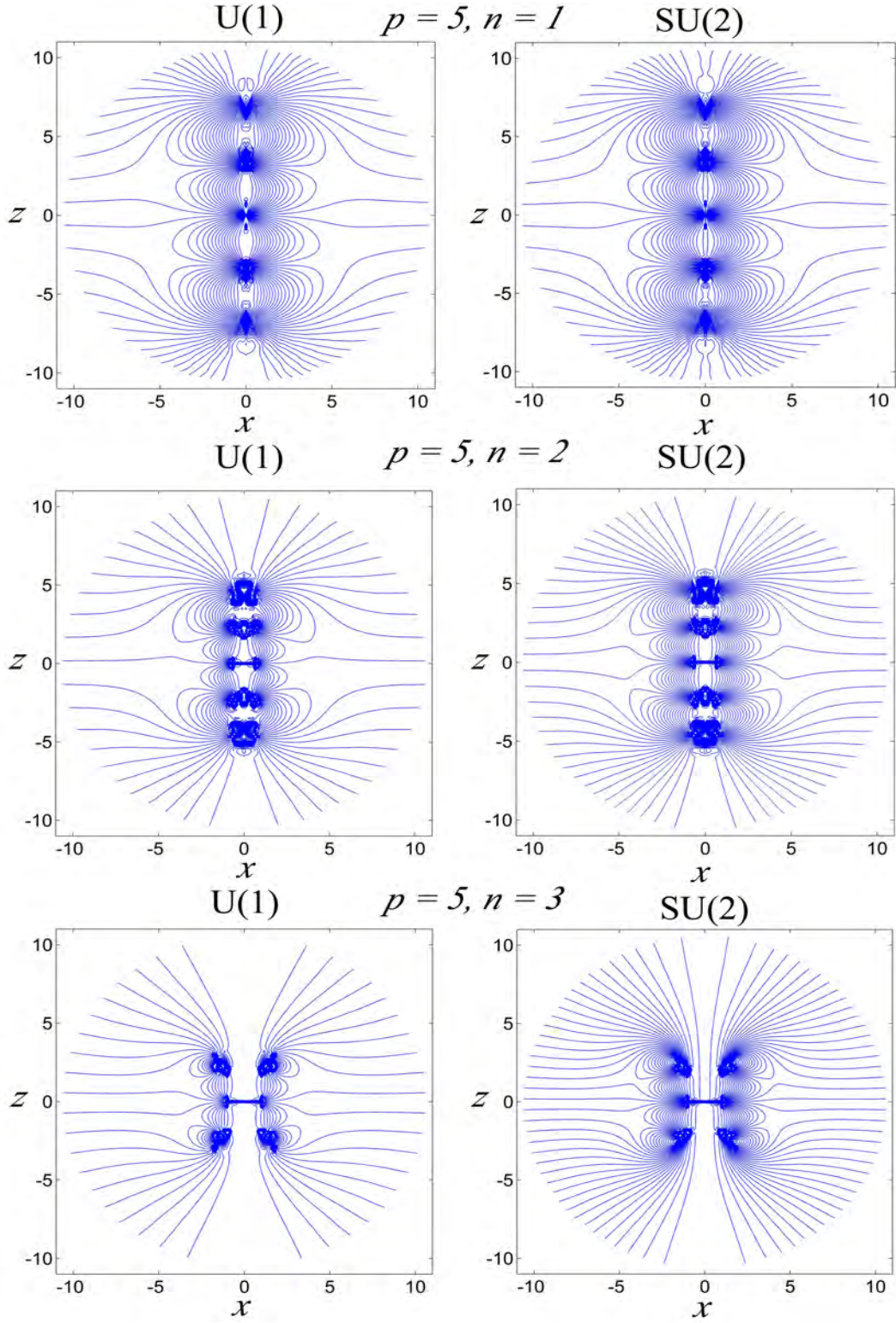


Figure 4: The contour line plot of the U(1) and SU(2) magnetic field lines for the MAMAM configurations along the x - z plane when $n = 1, 2$ and 3 .

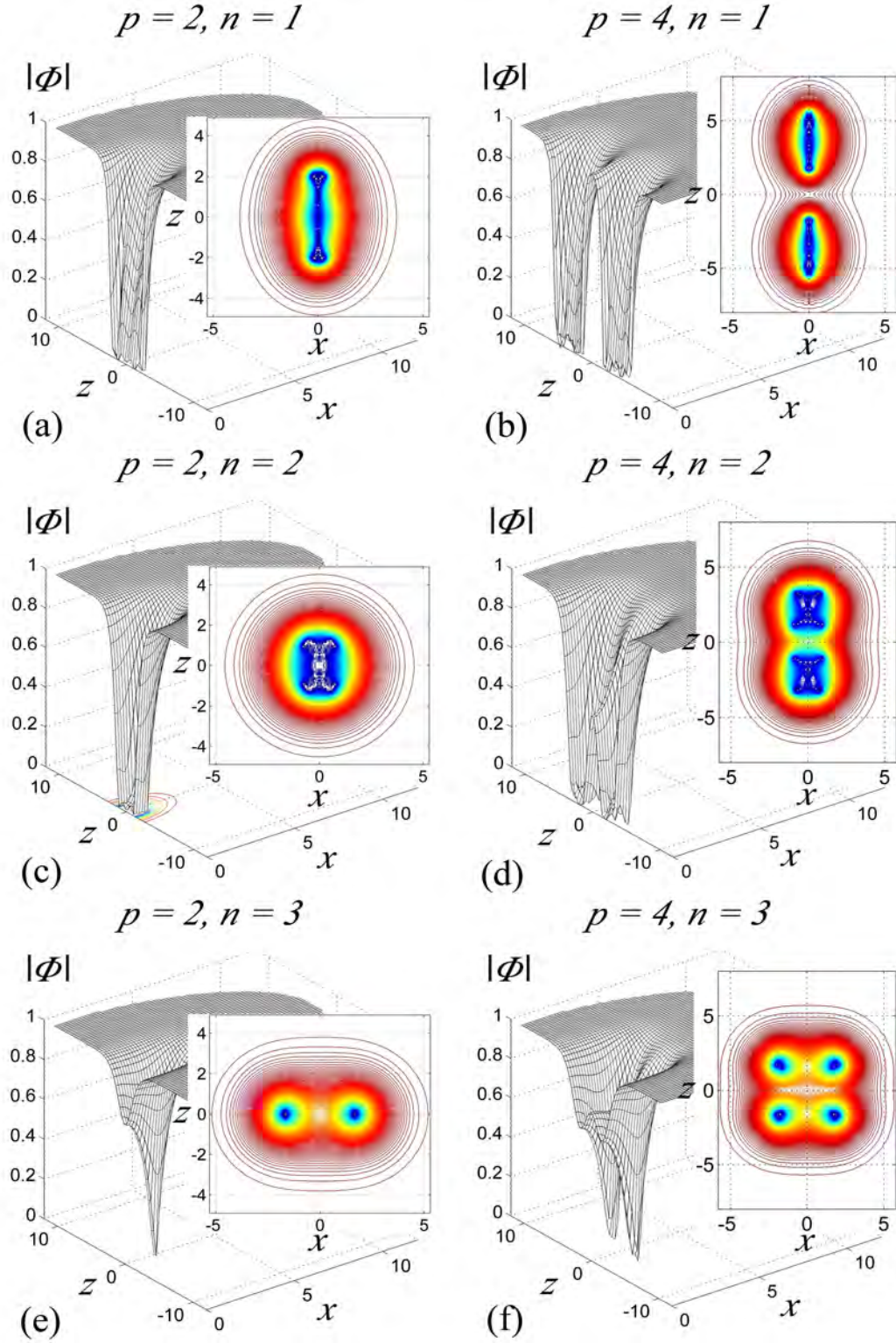


Figure 5: The 3-D and contour line plots of the Higgs field modulus Φ along the x - z plane for the MAP configurations when (a) $p = 2, n = 1$, (b) $p = 4, n = 1$, (c) $p = 2, n = 2$, (d) $p = 4, n = 2$, (e) $p = 2, n = 3$, and (f) $p = 4, n = 3$.

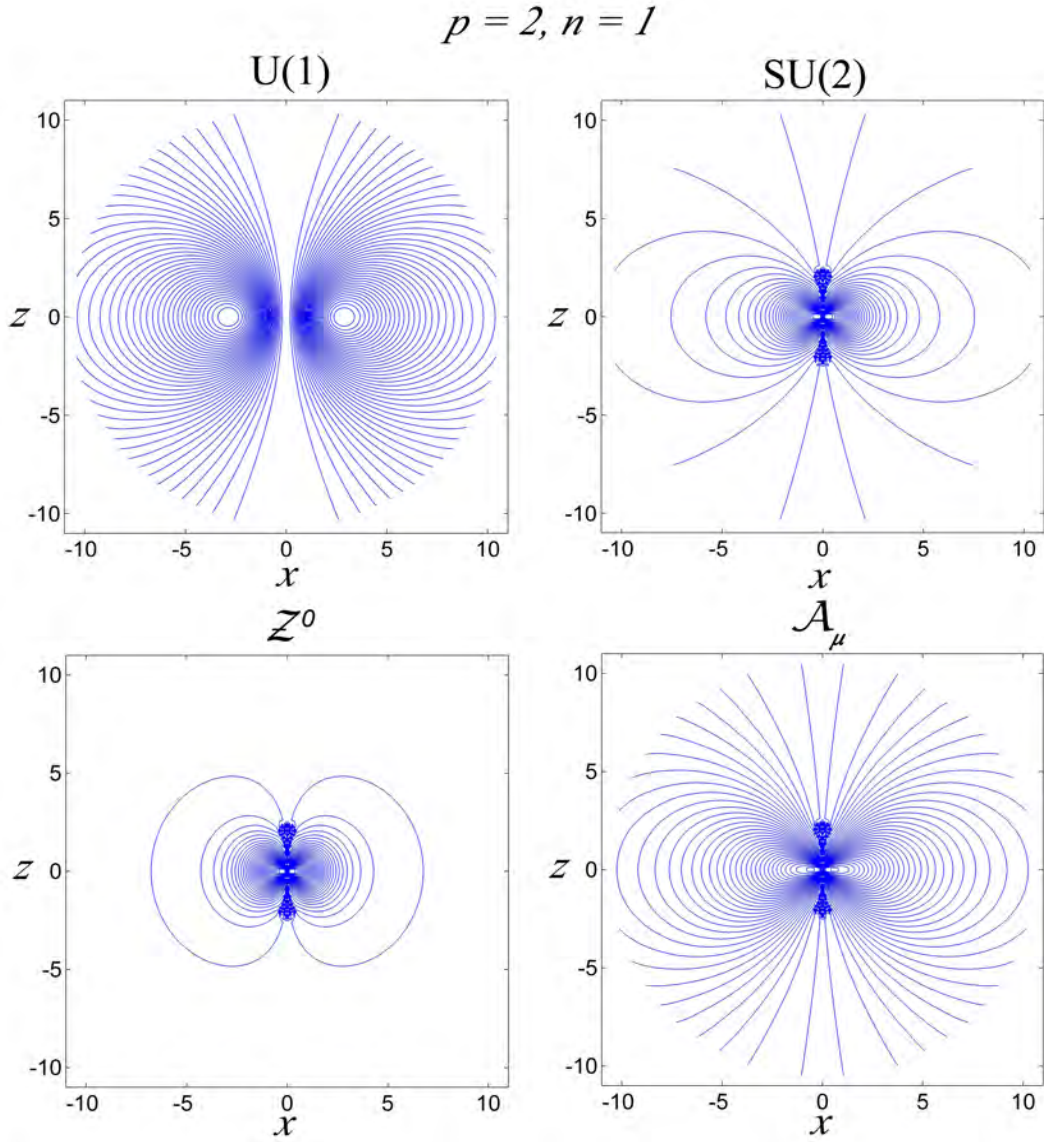


Figure 6: The contour line plot of the U(1), SU(2), neutral Z^0 , and electromagnetic \mathcal{A}_μ magnetic field lines for the 1-MAP configuration along the x - z plane when $p = 2$, $n = 1$ and $\theta_W = \frac{\pi}{6}$ rad.

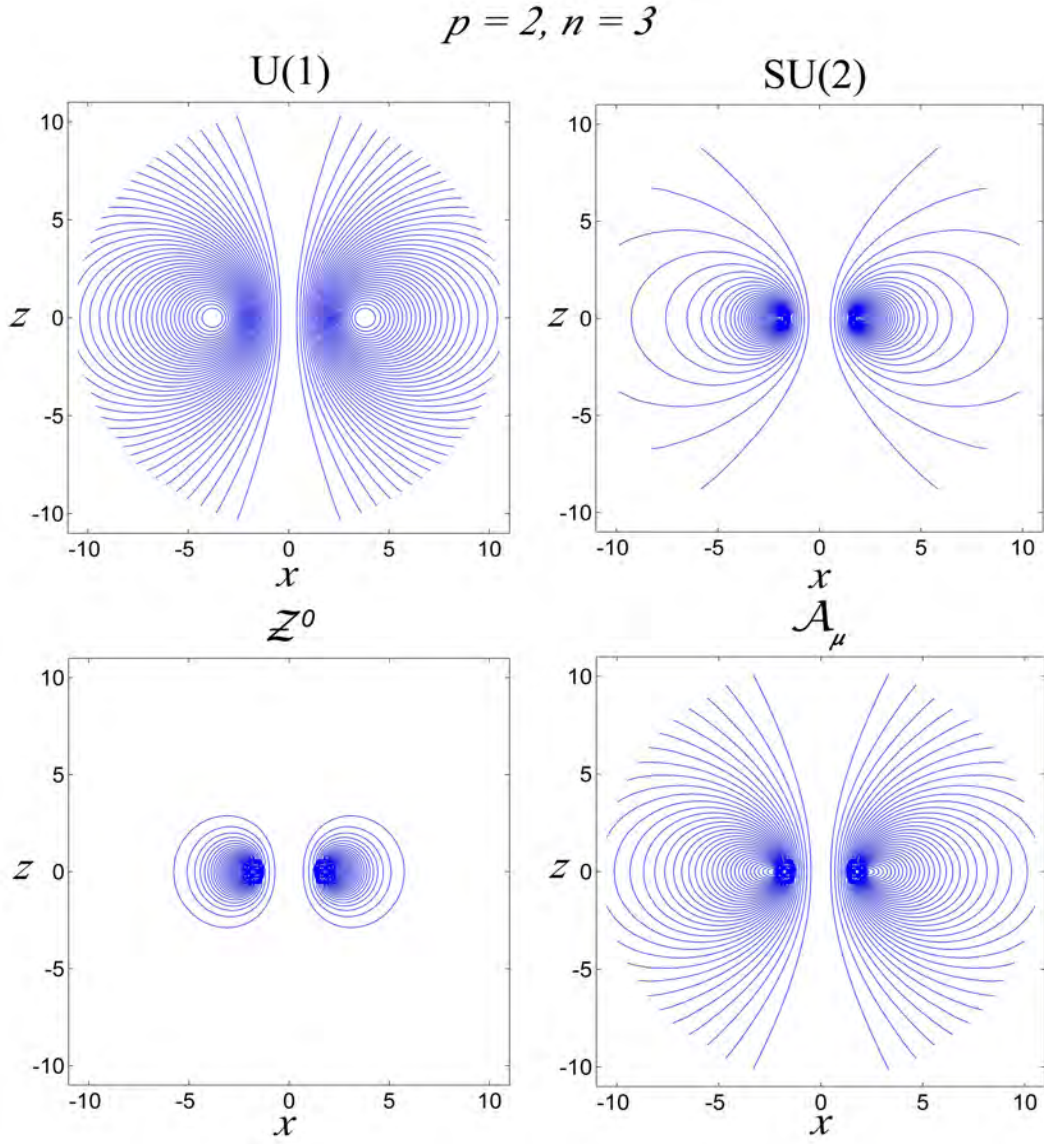


Figure 7: The contour line plot of the U(1), SU(2), neutral Z^0 , and electromagnetic \mathcal{A}_μ magnetic field lines for the 1-MAP configuration along the x - z plane when $p = 2$, $n = 3$ and $\theta_W = \frac{\pi}{6}$ rad.

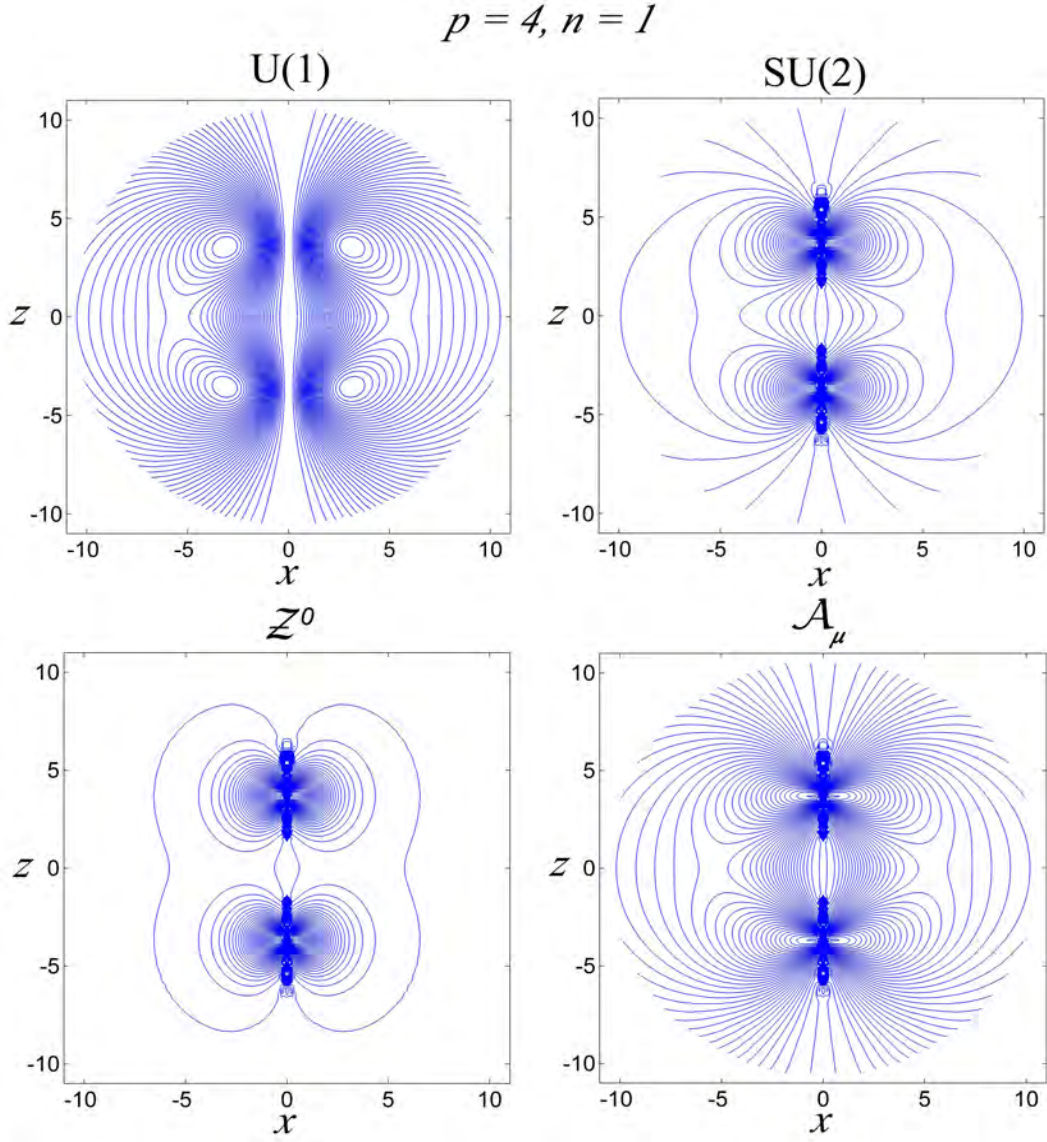


Figure 8: The contour line plot of the U(1), SU(2), neutral Z^0 , and electromagnetic \mathcal{A}_μ magnetic field lines for the 2-MAP configuration along the x - z plane when $p = 4$, $n = 1$ and $\theta_W = \frac{\pi}{6}$ rad.

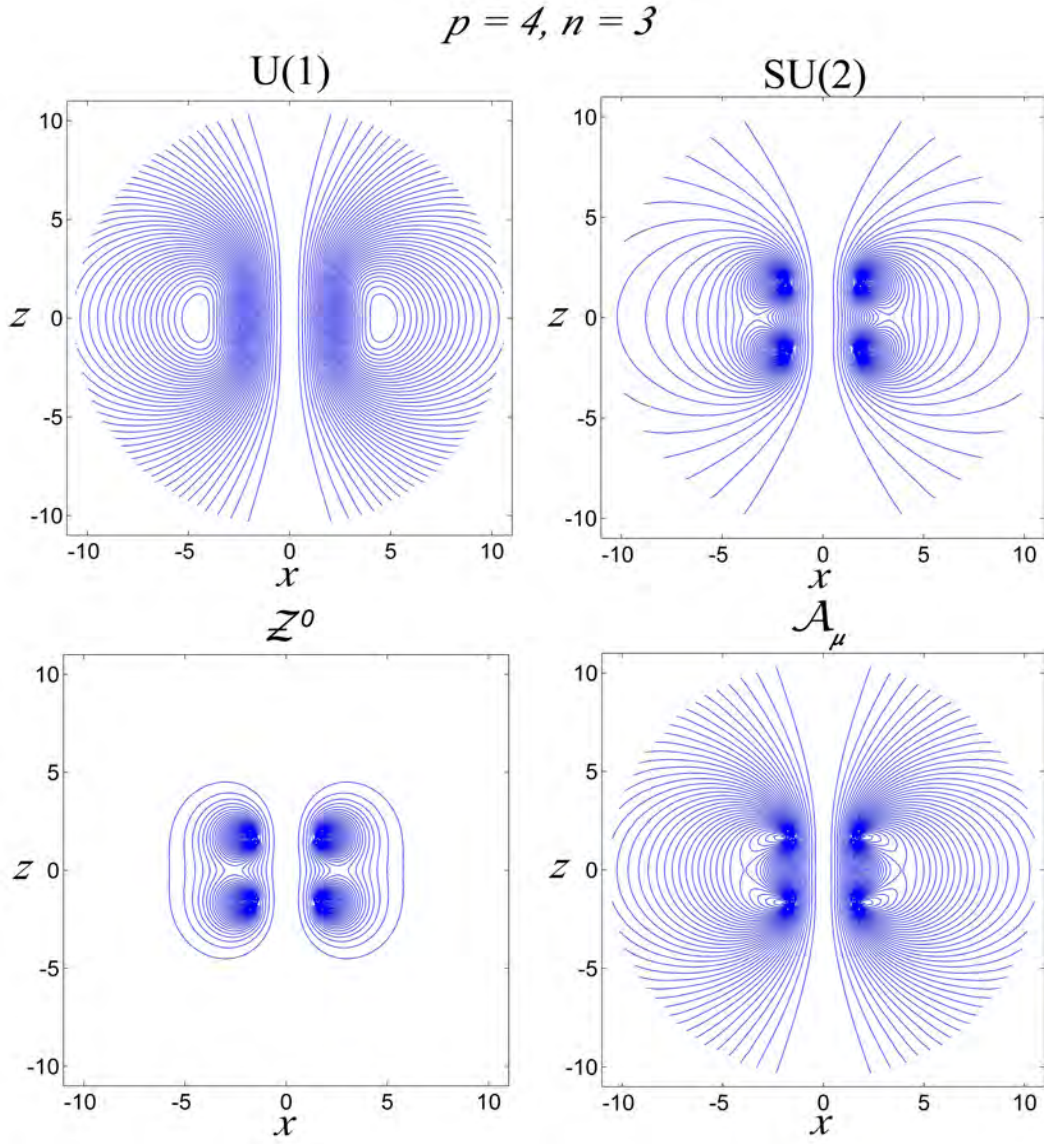


Figure 9: The contour line plot of the U(1), SU(2), neutral Z^0 , and electromagnetic \mathcal{A}_μ magnetic field lines for the 2-MAP configuration along the x - z plane when $p = 4$, $n = 3$ and $\theta_W = \frac{\pi}{6}$ rad.